RSC Advances

PAPER

View Article Online
View Journal | View Issue

Cite this: *RSC Adv.*, 2023, **13**, 9924

Magnetization reversal of perpendicular magnetic anisotropy regulated by ferroelectric polarization in $CoFe_3N/BaTiO_3$ heterostructures: first-principles calculations

Zirun Li, * Bo Chen, Shimin Shan and Yongmei Zhang

Exploring the electric-field switching of perpendicular magnetic anisotropy (PMA) in multiferroic heterostructures has important physical significance, which attracts great interest due to its promising application for energy-efficient information storage. Herewith, we investigate the effect of ferroelectric polarization on magnetic anisotropy in $CoFe_3N/BaTiO_3$ heterostructures using first-principles calculations. The calculations reveal that the magnetic anisotropy of $CoFe_3N$ can be regulated by ferroelectric polarization of $BaTiO_3$. When the ferroelectric polarization reverses, the PMA of FeCo–TiO_2 and FeN–BaO configurations remains, but in the FeN–TiO_2 and FeCo–BaO cases, magnetic anisotropy inverses between out-of-plane and in-plane direction. Further orbital-resolved analysis indicates that the transition of magnetic anisotropy is mainly attributed to the orbital hybridization of interfacial Fe/Co atoms with O atoms induced by the magnetoelectric effect. This study may open an effective approach toward modulating PMA and lays a foundation to the development of low energy consumption memory devices.

Received 21st March 2023
Accepted 29th March 2023

DOI: 10.1039/d3ra01842c

rsc.li/rsc-advances

Introduction

With the rapid development of information technology and the continuous advancement of spintronics, perpendicular magnetic anisotropy (PMA) has attracted intensive attention with potential application in energy-efficient information memory.[1–3] PMA is beneficial to obtain higher storage density, higher thermal stability and lower critical switching current density in non-volatile magnetic random access memory (MRAM).[4–6] PMA mainly arises at ferromagnetic/oxide interfaces, such as Fe/MgO,[6,7] CoFeB/MgO,[5] CoFeB/$BaTiO_3$,[8] Mn_3Ga/$SrTiO_3$,[9] and $(Co/Pt)_3$/PMN-PT.[10] It is also interesting that the magnetism of memory devices could be controlled by using an electric field through magnetoelectric (ME) coupling in multiferroic heterostructures. The ME effect at ferromagnetic/ferroelectric heterostructures also reduces the energy dissipation by Joule heating, which becomes another hot topic of information memory.[11–15] Various mechanisms on ME effect have been proposed and confirmed, such as strain,[16,17] charge,[18] and exchange-coupling.[19–21] More importantly, multiferroic heterostructures with PMA provide more effective method for achieving the magnetization switching *via* electric field, which will not only save energy consumption, but also expand the future application for non-volatile MRAM device.[22,23]

Among ferromagnets, anti-perovskite material Fe_4N has been reported as a very attractive candidate for spintronics applications due to high spin polarization, small coercivity and high Curie temperature.[24–26] In our previous experiment, epitaxial Fe_4N films can be grown on MgO, PMN-PT, and $SrTiO_3$ substrates and they all exhibit good interface and magnetic properties.[27–29] Experiment results show that the ME effect and magnetic anisotropy of Fe_4N/PMN-PT heterostructure can be tailored by electric field,[27,30] further confirmed by theoretical calculation.[31] $Fe_4N/MgO/Fe_4N$ magnetic tunnel junction (MTJ) has been predicted to produce an ultrahigh tunnel magnetoresistance (TMR),[32] Fe_4N/Alq_3/Co and LSMO/C_{60}/Fe_4N-MTJs exhibit a negative TMR and a regulable interface.[33,34] PMA has been obtained in $Fe_4N/BiFeO_3$, Fe_4N/MgO, and Fe_4N/PMN-PT heterostructure and it also can be tuned by strain, interfacial oxidation, ferroelectric polarization, and electric field.[31,35–38] However, the electric field switching of PMA does not achieve in Fe_4N-based heterostructure by ferroelectric polarization. Bulk Fe_4N is cubic symmetry and it does not have PMA, but the substitution of Co in the Fe_4N lattice induces a large PMA of tetragonal $CoFe_3N$.[39] By adsorbing organic molecules, organic/$CoFe_3N$ spinterface exhibits enhanced PMA.[40] Moreover, the Mn-substitution doping at the interfacial Fe_{II} position in the $Fe_4N/BaTiO_3$ heterostructure may obtain a large ME effect.[41] In order to further improve the interfacial PMA and achieving the electric field switching of PMA, the substitute $CoFe_3N$ is introduced as the ferromagnetic layer of multiferroic

School of Semiconductor and Physics, North University of China, Taiyuan 030051, China. E-mail: lizirun@nuc.edu.cn

heterostructure, which has a great application prospect for spintronics.

In this work, we construct the $CoFe_3N/BaTiO_3$ multiferroic heterostructures and investigate the impact of ferroelectric polarization on magnetic anisotropy using first-principles calculations. Our studies indicate that the magnetic anisotropy of $CoFe_3N$ can be regulated by ferroelectric polarization of $BaTiO_3$. Ferroelectric polarization reversal makes flipping of magnetization between the out-of-plane and in-plane direction in FeN–TiO_2 and FeCo–BaO interface configurations. Further orbital-resolved analysis indicates that the transition of magnetic anisotropy is mainly due to the strong interfacial ME coupling and orbital hybridization between interfacial Fe/Co atom and O atom. These results lay the foundation for realizing electric-field control of PMA in multiferroic heterostructures.

Computational details and models

First-principles calculations are carried out based on density functional (DFT) theory using Vienna *Ab initio* Simulation Package code.[42–44] Exchange and correlation effects are accounted for by the generalized gradient approximation (GGA) as parameterized by Perdew, Burke, and Ernzerhof (PBE).[45] Although the PBE functional has an overestimation for unit cell volume,[46] extensive studies demonstrate that it is suitable for the study of multiferroic heterostructure.[17,47,48] Structural relaxations are performed until the force becomes less than 10^{-2} eV Å^{-1} and the change in the total energy between two ionic relaxation steps is smaller than 10^{-5} eV. An energy cutoff of 500 eV and $9 \times 9 \times 9$, $11 \times 11 \times 1$ *k*-point meshes are used for the bulk and heterostructures, respectively. The $CoFe_3N/BaTiO_3$ heterostructures comprise seven-layered $CoFe_3N$ and seven-layered $BaTiO_3$, followed by a 15 Å vacuum layer. The experimental lattice constant of bulk $BaTiO_3$ is 3.99 Å and the in-plane lattice constant of bulk $CoFe_3N$ is 3.78 Å,[39] which has a lattice mismatch of 5.3%. Here, we build the $CoFe_3N/BaTiO_3$ heterostructures is based on the previous experiment research of Fe_4N/oxide heterostructure.[27,28,30] The binding energy (E_B) calculation is preformed to display the structural stability of different interface configurations. The magnetic anisotropy energy (MAE) is determined using the magnetic force theorem with spin–orbit coupling (SOC).[49–51] The MAE depends on the nonzero coupling matrix element between the occupied and unoccupied d-orbital states.[51] The total MAE values of $CoFe_3N/BaTiO_3$ heterostructures are calculated from the energy difference between the magnetic moment aligning in the in-plane (*x* axis) and out-of-plane (*z* axis) orientations. The positive value of MAE represents PMA and negative value represents in-plane magnetic anisotropy (IMA).

Results and discussion

Prior to investigating the regulated magnetic anisotropy by ferroelectric polarization, we first discuss the properties of bulk $CoFe_3N$ and $BaTiO_3$, as shown in Fig. 1. In tetragonal $CoFe_3N$, the corner site is occupied by Fe atom, named it Fe_I, the Fe atoms at face-centered site are named by Fe_{II}, and another face-centered site is occupied by Co atom, as shown in Fig. 1(a). The strong hybridization between Fe_{II} and N atoms makes distinct density of states in Fe_I and Fe_{II} atoms,[32,52] so Fe_I and Fe_{II} atoms exhibit outstanding difference in magnetic properties. In bulk $CoFe_3N$, the magnetic moments of Fe_I, Fe_{II}, and Co atoms are 2.987 μ_B, 2.229 μ_B, and 1.180 μ_B, respectively. In Fig. 1(c), the MAE results of $CoFe_3N$ show that Fe_I, Fe_{II}, and Co atoms have a noticeable difference. Fe_I atom has an IMA contribution whereas Fe_{II} atom exhibits a PMA. Furthermore, Co atom shows a large PMA of 0.319 meV. We then display the orbital-resolved MAE of Fe and Co atoms in Fig. 1(d)–(f) to analysis the orbital contribution for MAE. In Fe_I, nonzero coupling matrix element $\langle x^2-y^2|\hat{L}_z|xy\rangle$ favors IMA, but it turns to support PMA in Fe_{II} and Co atoms. The difference in chemical environment of Fe_I, Fe_{II}, and Co atoms determines the d-orbital distribution near the Fermi level,[32,38,52] finally altering the magnetic moment and MAE of Fe and Co atoms. Fig. 1(g) displays the total density of states (DOS) and partial DOS of bulk $CoFe_3N$. The results show that there is spin majority states of Fe_{II} and Co atoms pass through the Fermi level whereas there are not spin majority d states near the Fermi level in Fe_I atom, which leads to the distinct magnetic properties. Fig. 1(b) shows that bulk $BaTiO_3$ has a typical perovskite structure and the DOS result in Fig. 1(h) indicates that it is a non-magnetic insulator.[53]

We then built $CoFe_3N/BaTiO_3$ heterostructures with ideal interface, and complex interface situations such as oxygen diffusion, disorder, and lattice distortion are not considered in this work. Four possible ideal interface structures are taken into account, namely, FeCo–TiO_2, FeN–TiO_2, FeCo–BaO, and FeN–BaO type interface, as shown in Fig. 2. The grey arrows indicate the polarization direction of $BaTiO_3$. The positive ferroelectric polarization along the *z* axis is pointing away from the $BaTiO_3$. It should be pointed that interfacial Fe atom in FeCo termination is Fe_I and interfacial Fe atom in FeN termination is Fe_{II}. In order to explore the influence of interface structure on magnetic anisotropy, we first analyze the interface bonding and structure difference. In FeCo–TiO_2 configuration, interfacial Co atom occupies atop sites on Ti atom. Polarization reversal makes the interfacial Co atom shift away from the interface. In FeN–TiO_2 configuration, interfacial Fe_{II} atom bonds with O atom. Such a Fe–O bond leads to d-orbital reconstruction, which in turn affects the magnetic properties of $CoFe_3N$ part with the presence of ferroelectric polarization. Intriguingly, interfacial Co and O atoms are bonded strongly and the bond length is only 1.811 Å in FeCo–BaO ($P_\downarrow$) case, making the overlap between Co-3d and O-2p states stronger, whereas Co and O atoms are far away from each other in FeCo–BaO ($P_\uparrow$) case. In FeN–BaO configuration, regardless of polarization direction, they all exhibit a large interface distance. The significant change of interface structure with the process of polarization reversal may cause the change in electronic structure, spin magnetism, and MAE.[53,54]

In Table 1, we first list the E_B of $CoFe_3N/BaTiO_3$ heterostructures with different configurations to determine the stability of heterostructures, which is defined as $E_B = E_{CoFe_3N/BaTiO_3} - E_{CoFe_3N} - E_{BaTiO_3}$. E_{CoFe_3N} and E_{BaTiO_3} represent the

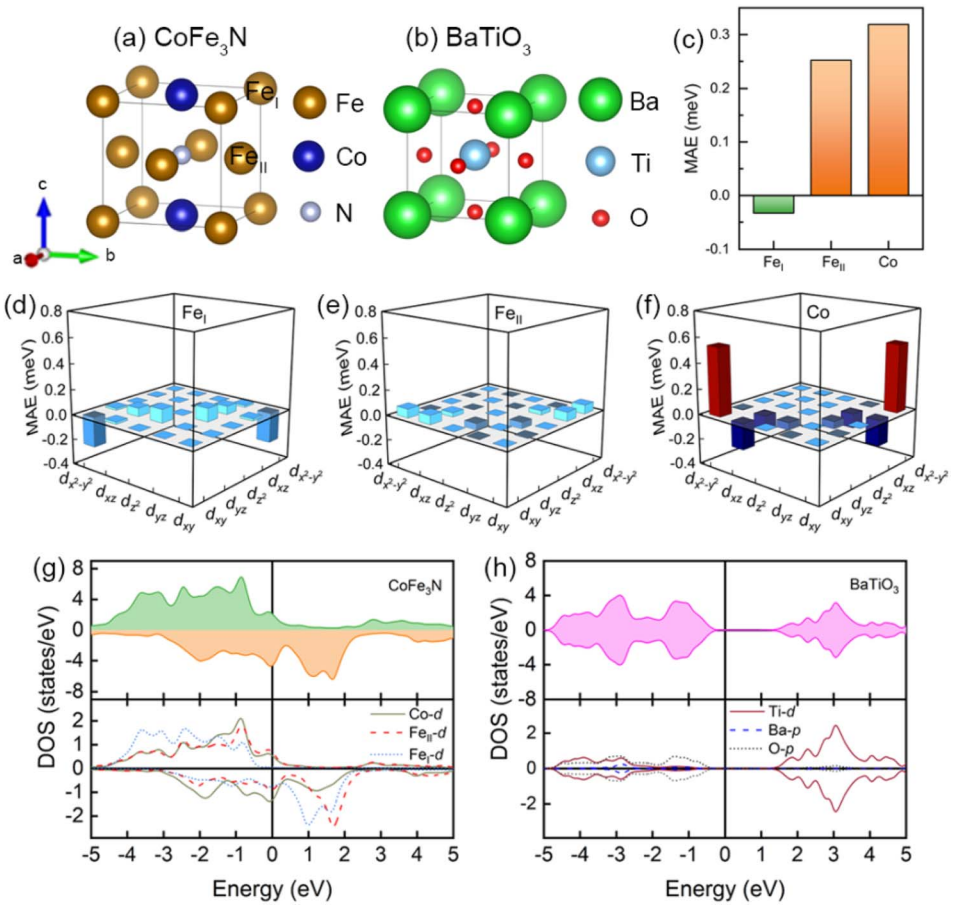

Fig. 1 (a) and (b) The lattice structure of bulk $CoFe_3N$ and $BaTiO_3$. (c) MAE of Fe and Co atoms in bulk $CoFe_3N$. (d)–(f) Orbital-resolved MAE of Fe and Co atoms in bulk $CoFe_3N$. (g) and (h) Total and partial density of states (DOS) of bulk $CoFe_3N$ and $BaTiO_3$.

energies of the surface of $CoFe_3N$ part and $BaTiO_3$ part, and $E_{CoFe_3N/BaTiO_3}$ is the total energy of $CoFe_3N/BaTiO_3$ heterostructure.[47,53] The negative E_B indicates that FeCo–BaO and FeN–TiO_2 configurations are experimentally feasible. FeCo–TiO_2 ($P_\uparrow$) and FeN–BaO ($P_\downarrow$) configurations have positive values, indicating the process of polarization reversal may affect the interface stability.

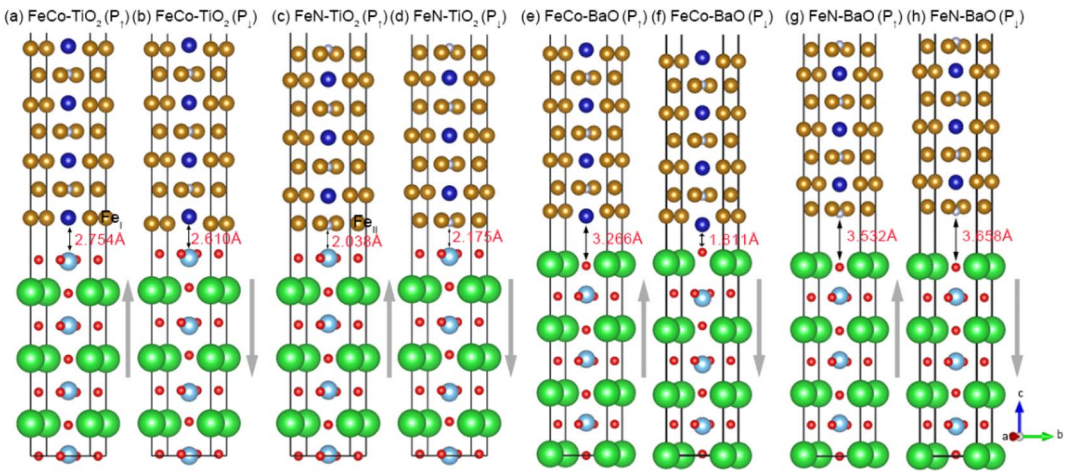

Fig. 2 The $CoFe_3N/BaTiO_3$ heterostructures with different configurations. (a) and (b) FeCo–TiO_2, (c) and (d) FeN–TiO_2, (e) and (f) FeCo–BaO, and (g) and (h) FeN–BaO. The grey arrows indicate the polarization direction of $BaTiO_3$. The interfacial Fe and Co atoms and interface distance are marked.

Table 1 E_B (eV), magnetic moment (μ_B), and MAE (mJ m^{-2}) of $CoFe_3N/BaTiO_3$ heterostructures with different configurations

Configuration	E_B	$\mu_s^{Ti/Ba}$	μ_s^{O}	$\mu_s^{Fe_I/Fe_{II}}$	μ_s^{Co}	MAE
FeCo–TiO_2 ($P_\uparrow$)	0.181	−0.229	0.012	3.114	1.206	0.978
FeCo–TiO_2 ($P_\downarrow$)	−0.062	−0.116	0.012	3.251	−0.562	1.138
FeN–TiO_2 ($P_\uparrow$)	−2.476	−0.025	0.056	2.610	—	−0.043
FeN–TiO_2 ($P_\downarrow$)	−1.302	0.006	0.049	2.646	—	5.139
FeCo–BaO ($P_\uparrow$)	−0.338	−0.006	−0.158	2.956	1.257	0.894
FeCo–BaO ($P_\downarrow$)	−1.336	0.016	0.158	2.846	1.591	−0.181
FeN–BaO ($P_\uparrow$)	−0.367	−0.001	−0.138	2.476	—	2.532
FeN–BaO ($P_\downarrow$)	1.005	−0.000	0.004	2.467	—	1.958

Table 1 also gives the magnetic moments of the interfacial Ti, Ba, O, Fe, and Co atoms in $CoFe_3N/BaTiO_3$ heterostructures with $P_\uparrow$ and $P_\downarrow$. The appearance of magnetic moment in Ti and O atoms can be attributed to the orbital hybridization with Fe/Co atom, which demonstrates strong ME effect at the interface.[48,55] In FeCo–TiO_2 configuration, the magnetic moment of Fe_I atom has a marked increase compared to the bulk $CoFe_3N$, owing to the strong Fe 3d and O 2p orbital hybridization. The polarization reversal gives rise to an inversion of Co magnetic moment from 1.206 μ_B ($P_\uparrow$) to −0.562 μ_B ($P_\downarrow$), indicating that the magnetic structure can be regulated by $BaTiO_3$ polarization. In FeN–TiO_2 configuration, the magnetic moment of Fe_{II} atom has a tiny change with the polarization reversal. In FeCo–BaO configuration, the magnetic moment of O atom can be switched from parallel to antiparallel to the Co atom. This means that a strong ME coupling is formed in FeCo–BaO configuration, which has a good application prospect in spintronics. In addition, the total MAEs of $CoFe_3N/BaTiO_3$ heterostructures are also shown in Table 1. For FeN–TiO_2 and FeCo–BaO configuration, by changing the polarization direction, the easy magnetic axis is switched between out-of-plane direction and in-plane direction. Especially, in FeN–TiO_2 configuration, negative polarization makes the PMA increase significantly, confirming that polarization reversal produces a sizable change in magnetic anisotropy. However, regardless of polarization direction, PMA remains in FeCo–TiO_2 and FeN–BaO configurations.

To further clarify the origin of MAE, layer-resolved MAEs are shown in Fig. 3(a) and (b). For both polarization directions, MAE changes mainly in the interfacial and surface layer, owing to the anisotropic nature resides at the interface or surface.[48] In Fig. 3(a), interfacial MAE has a sharp decline in FeCo–TiO_2 configuration when the magnetoelectric effect is applied as $P_\uparrow \rightarrow P_\downarrow$. In FeN–$TiO_2$ configuration, the magnitude of MAE in every layer has an increase with the polarization reversal. In Fig. 3(b), FeCo–BaO configurations with $P_\uparrow$ and $P_\downarrow$ states exhibit distinct trends in interfacial MAE, being positive and negative in sign, respectively. This indicates that the magnetization direction can reorient from out-of-plane easy axis to in-plane by reversing the polarization direction. In FeN–BaO configuration, interfacial MAE is almost unchanged as $P_\uparrow \rightarrow P_\downarrow$. Further, to get more insights, we analyze the atom-resolved MAE of interfacial Fe and Co atoms, as shown in Fig. 3(c) and (d). The interfacial Fe/Co atom plays an important role in the electronic structure near the Fermi level and interfacial magnetic anisotropy. In FeCo–TiO_2 configuration, the MAE of Fe_I and Co atoms decrease severely. In FeN–TiO_2 configuration, both Fe_{II} atoms favor the PMA and PMA increases at $P_\downarrow$ state. In FeCo–BaO configuration, Fe_I favors PMA and yet Co supports IMA, which is contrary to the bulk $CoFe_3N$. When the polarization reverses, the opposite MAE of Fe_I and Co atoms brings about the changed sign of interfacial MAE. In FeN–BaO configuration, the MAE of interfacial Fe_{II} atoms changes little during $P_\uparrow \rightarrow P_\downarrow$.

To elucidate the effect of interfacial structure and polarization reversal on PMA, we show the d-orbital-resolved MAE of interfacial Fe and Co atoms in Fig. 4. According to the second-

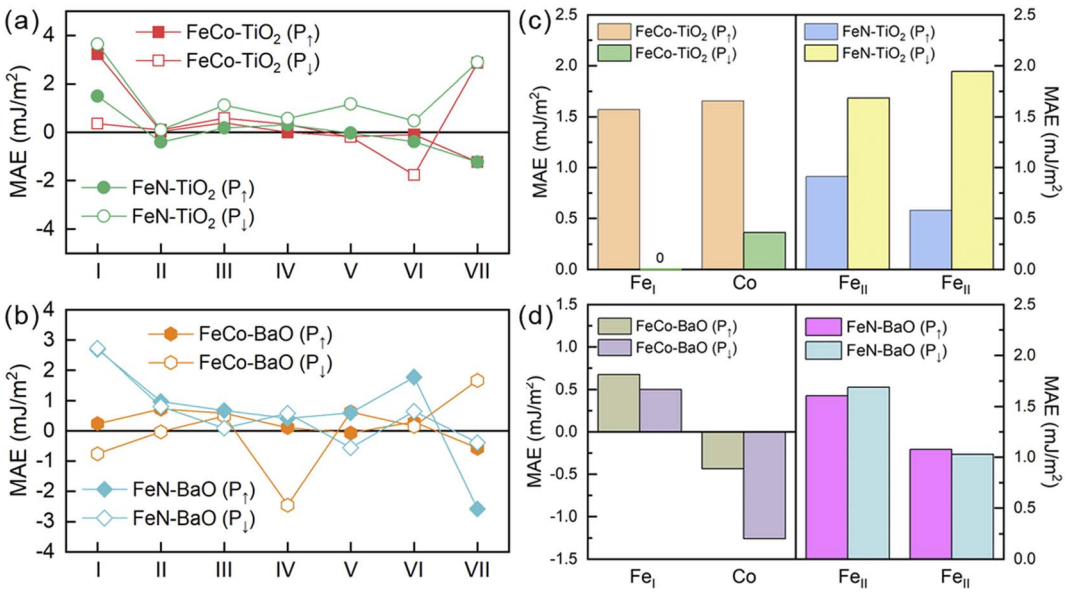

Fig. 3 (a) and (b) The layer-resolved MAE of $CoFe_3N/BaTiO_3$ heterostructures with TiO_2 and BaO terminations. (c) and (d) The MAE of interfacial Fe and Co atoms of $CoFe_3N/BaTiO_3$ heterostructures with TiO_2 and BaO terminations.

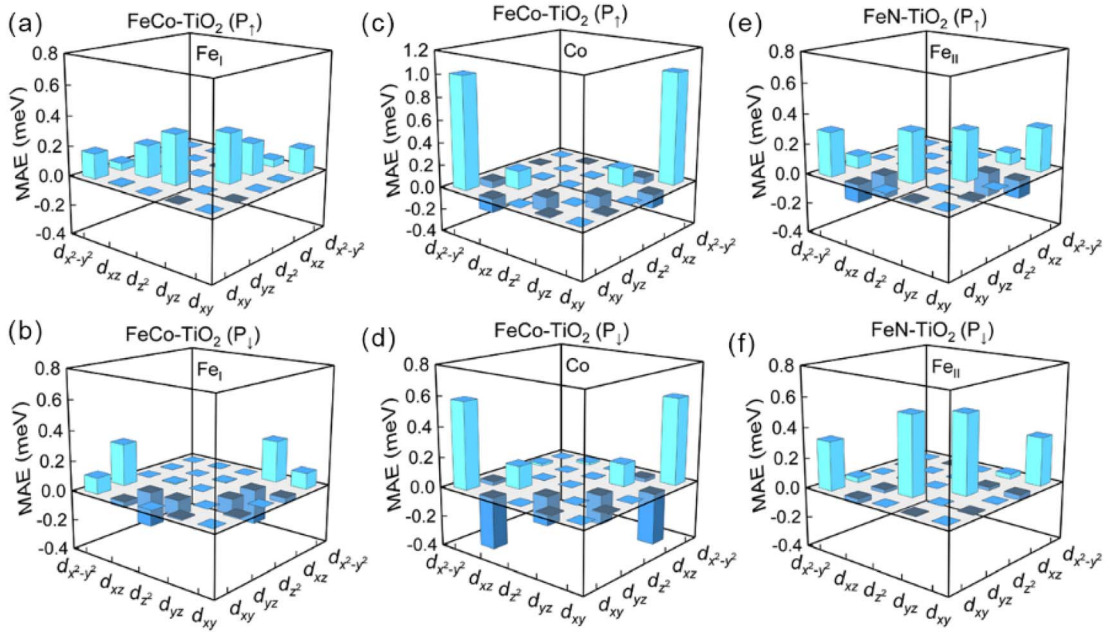

Fig. 4 The orbital-resolved MAE of interfacial Fe and Co atoms in $CoFe_3N/BaTiO_3$ heterostructures with TiO_2 termination. (a) and (b) Fe_I of FeCo-TiO_2, (c) and (d) Co of FeCo-TiO_2, (e) and (f) Fe_{II} of FeN-TiO_2.

order perturbation theory,[50,51] the MAE depends on the nonzero coupling matrix element between the occupied and unoccupied d-orbital states. The MAE can be defined as $\mathrm{MAE} \propto \xi^2 \sum_{o,u} \frac{|\langle \psi_o|\hat{L}_z|\psi_u\rangle|^2 - |\langle \psi_o|\hat{L}_x|\psi_u\rangle|^2}{E_u - E_o}$, where ψ_o and ψ_u indicate the occupied and unoccupied states with the energies E_o and E_u, respectively. ξ is the SOC constant. $\hat{L}_{z(x)}$ is the $z(x)$ component of the orbital angular momentum operator. These nonzero coupling matrix elements include $\langle xz|\hat{L}_z|yz\rangle = 1$, $\langle x^2-y^2|\hat{L}_z|xy\rangle = 2$, $\langle z^2|\hat{L}_x|yz\rangle = 3$, $\langle xy|\hat{L}_x|xz\rangle = 1$, and $\langle x^2-y^2|\hat{L}_x|yz\rangle = 1$.[50]

Meanwhile, in order to better explain the PMA contribution of matrix elements, we analyze the DOS of interfacial Fe and Co atoms from the d-orbital perspective in Fig. 6. In FeCo–TiO_2 ($P_\uparrow$) case, for Fe_I atom, all nonzero matrix elements provide the positive contribution to MAE. Among them, the contribution of

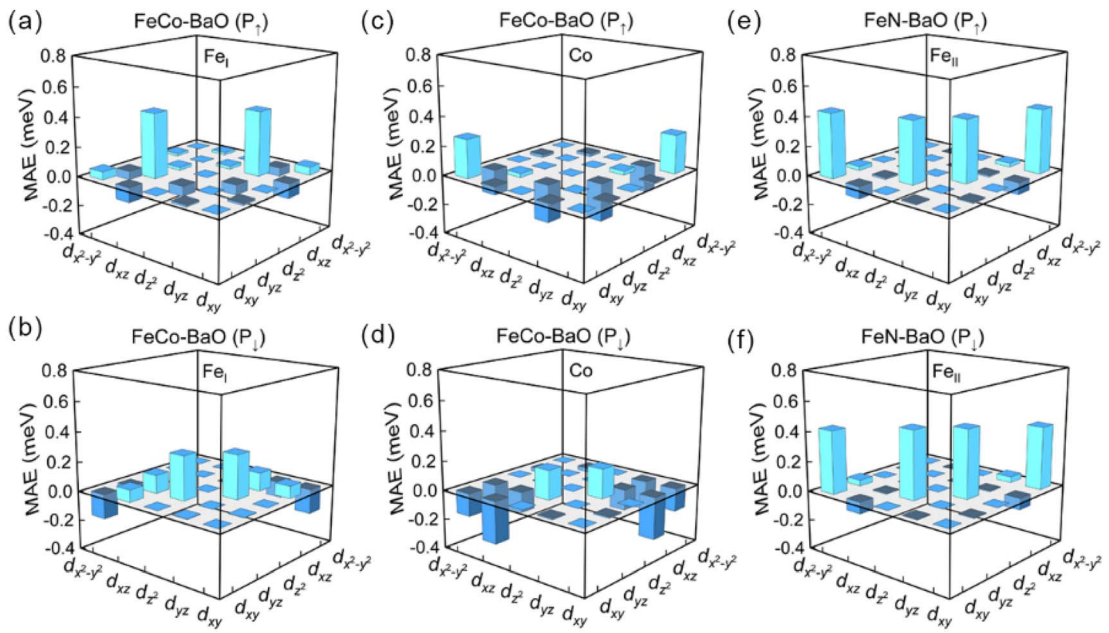

Fig. 5 The orbital-resolved MAE of interfacial Fe and Co atoms in $CoFe_3N/BaTiO_3$ heterostructures with BaO termination. (a) and (b) Fe_I of FeCo-BaO, (c) and (d) Co of FeCo-BaO, (e) and (f) Fe_{II} of FeN-BaO.

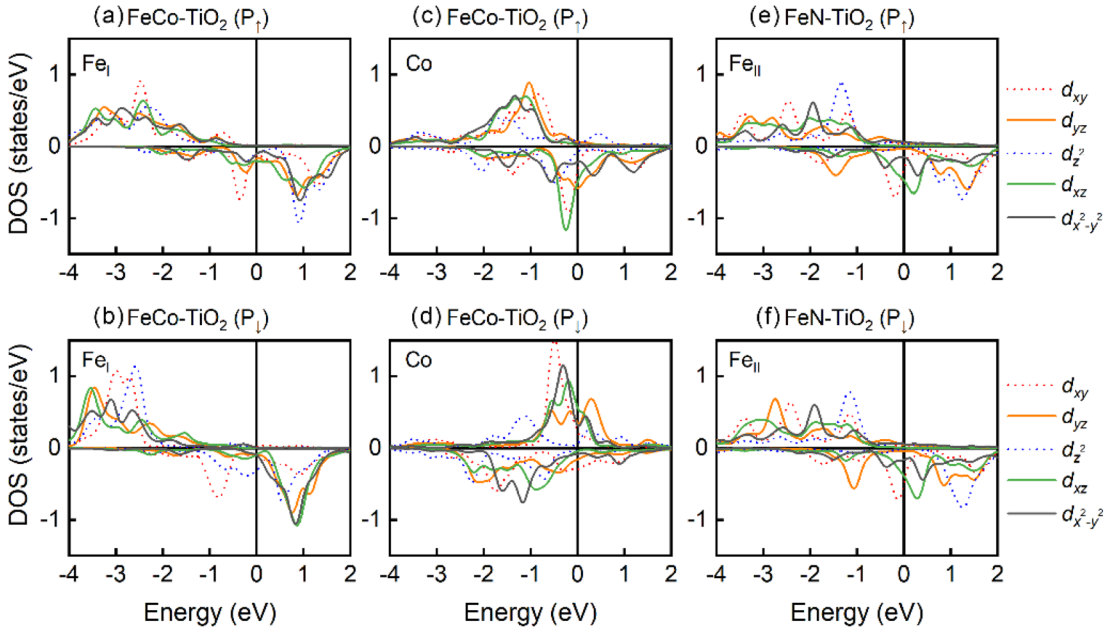

Fig. 6 The DOS of interfacial Fe and Co atoms in $CoFe_3N/BaTiO_3$ heterostructures with TiO_2 termination. (a) and (b) Fe_I of FeCo-TiO_2, (c) and (d) Co of FeCo-TiO_2, (e) and (f) Fe_{II} of FeN-TiO_2.

$\langle z^2|\hat{L}_x|yz\rangle$ is the most and it favors PMA. In FeCo–TiO_2 ($P_\downarrow$) case, these two terms of $\langle z^2|\hat{L}_x|yz\rangle$ and $\langle xz|\hat{L}_z|yz\rangle$ turn to support IMA, which cancels out the PMA contribution and makes the MAE of Fe_I atom zero. According to DOS of Fig. 6(a) and (b), during the $P_\uparrow \rightarrow P_\downarrow$, spin majority electron in d_{yz} occupied states of Fe_I atom disappears, which produces the negative contribution of $\langle z^2|\hat{L}_x|yz\rangle$ and $\langle xz|\hat{L}_z|yz\rangle$ terms. For Co atom, the $\langle x^2-y^2|\hat{L}_z|xy\rangle$ matrix element always has a large PMA. However, the IMA contribution of $\langle xy|\hat{L}_x|xz\rangle$ increases as $P_\uparrow \rightarrow P_\downarrow$, causing the PMA of Co atom decreases, which is attributed to spin transition of d_{xz} occupied state near the Fermi level. In FeN–TiO_2 configuration, polarization reversal ($P_\uparrow \rightarrow P_\downarrow$) gives rise to the increase of PMA in interfacial Fe_{II} atom, which mainly comes from the growing PMA contribution of the matrix element $\langle z^2|\hat{L}_x|yz\rangle$ and the reduced IMA contribution of $\langle xz|\hat{L}_x|yz\rangle$ term. Based on the DOS of Fe_{II} atom, d_{yz} occupied state with spin

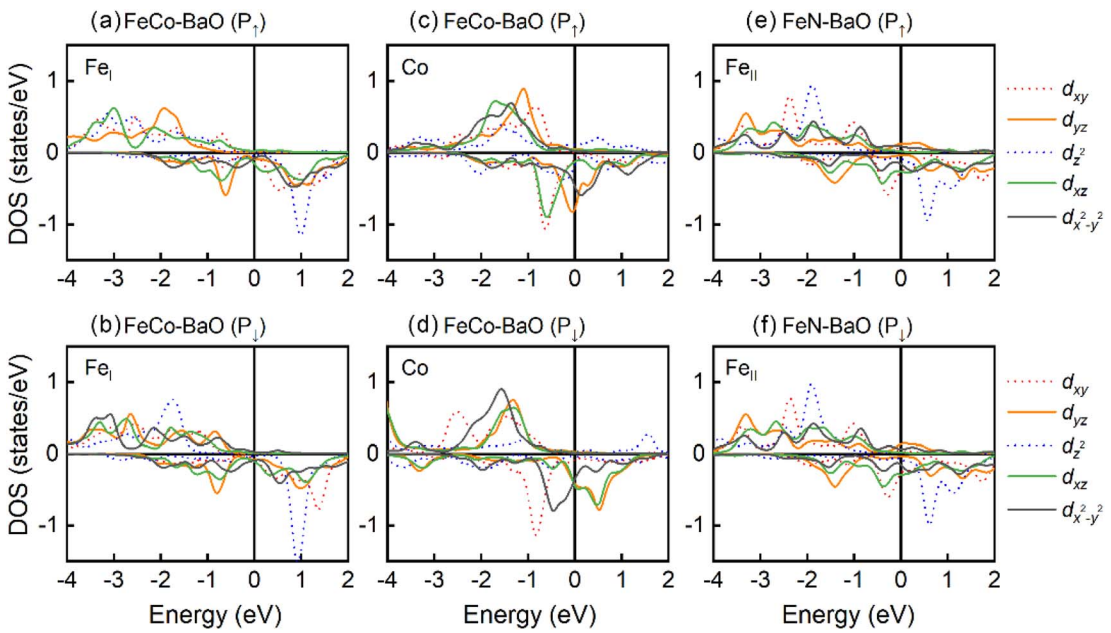

Fig. 7 The DOS of interfacial Fe and Co atoms in $CoFe_3N/BaTiO_3$ heterostructures with BaO termination. (a) and (b) Fe_I of FeCo-BaO, (c) and (d) Co of FeCo-BaO, (e) and (f) Fe_{II} of FeN-BaO.

down shifts to the Fermi level, decreasing the energy level difference and leading to the growing PMA contribution of the matrix element $\langle z^2|\hat{L}_x|yz\rangle$ and the reduce of IMA contribution of $\langle xz|\hat{L}_x|yz\rangle$. It suggests that the MAE of the Fe_{II} atom is more sensitive to the external condition, which is consistent with Fe_4N/MgO heterostructure.[38]

Fig. 5 and 7 give the d-orbital-resolved MAE and DOS of interfacial Fe and Co atoms in FeCo–BaO and FeN–BaO structures. In FeCo–BaO configuration, during the $P_\uparrow \rightarrow P_\downarrow$, most of zero matrix elements of Fe_I atom changes the sign, which is ascribed to the appearance of majority 3d electrons including d_{yz}, d_{z^2}, $d_{x^2-y^2}$ occupied states. Distinguishingly, the PMA contribution of $\langle x^2-y^2|\hat{L}_z|xy\rangle$ of Co atom is no longer the dominant, even the contribution of $\langle x^2-y^2|\hat{L}_z|xy\rangle$ turn into IMA with the polarization reversal. The inversion of MAE contribution of $\langle x^2-y^2|\hat{L}_z|xy\rangle$ comes from the disappearance of d_{xy} majority occupied states near the Fermi level. What's more, the MAE contributions of $\langle x^2-y^2|\hat{L}_x|yz\rangle$ and $\langle z^2|\hat{L}_x|yz\rangle$ terms are also changed in sign. On the basis of DOS result, the disappearance of d_{yz} minority occupied states plays a key role in the change of the MAE sign. In FeN–BaO termination, $\langle x^2-y^2|\hat{L}_z|xy\rangle$ and $\langle z^2|\hat{L}_x|yz\rangle$ of interfacial Fe_{II} atom have a positive contribution. The contribution of all matrix elements remains stable during the polarization reversal as a result of the weak ME coupling and unchanged DOS.

Conclusions

In summary, the effect of ferroelectric polarization on magnetic anisotropy in $CoFe_3N/BaTiO_3$ heterostructure has been demonstrated by first-principles calculations. We found that ferroelectric polarization reverses magnetic anisotropy of FeN–TiO_2 and FeCo–BaO configurations. The interfacial Fe_I, Fe_{II}, and Co atoms play a crucial role in determining the magnetic anisotropy of $CoFe_3N/BaTiO_3$ heterostructures, which is attributed to the orbital hybridization between interfacial Fe/Co atom and O atom due to the ME coupling effect. This work paves the way for nonvolatile electrical control of multiferroic heterostructure and applications in spintronics devices.

Author contributions

Zirun Li conducted first-principles calculations and drafted this paper. Bo Chen, Shimin Shan and Yongmei Zhang have taken part in the revision.

Conflicts of interest

There are no conflicts of interest to declare.

Acknowledgements

This work was supported by the National Natural Science Foundation of China (Grant No. 12204438), and the Shanxi Province Science Foundation for Youths (Grant No. 201901D211264), and the Fundamental Research Program of Shanxi Province (Grant No. 202103021224185 and 202203021212116), and the Scientific and Technological Innovation Programs of Higher Education Institutions in Shanxi (Grant No. 2020L0289), and the Science Foundation of North University of China (Grant No. XJJ201905).

References

1 I. Žutić, J. Fabian and S. D. Sarma, *Rev. Mod. Phys.*, 2004, **76**, 323–410.
2 C. Song, B. Cui, F. Li, X. J. Zhou and F. Pan, *Prog. Mater. Sci.*, 2017, **87**, 33–82.
3 S. Bhatti, R. Sbiaa, A. Hirohata, H. Ohno, S. Fukami and S. N. Piramanayagam, *Mater. Today*, 2017, **20**, 530–548.
4 B. Dieny and M. Chshiev, *Rev. Mod. Phys.*, 2017, **89**, 025008.
5 S. Ikeda, K. Miura, H. Yamamoto, K. Mizunuma, H. D. Gan, M. Endo, S. Kanai, J. Hayakawa, F. Matsukura and H. Ohno, *Nat. Mater.*, 2010, **9**, 721–724.
6 J. W. Koo, S. Mitani, T. T. Sasaki, H. Sukegawa, Z. C. Wen, T. Ohkubo, T. Niizeki, K. Inomata and K. Hono, *Appl. Phys. Lett.*, 2013, **103**, 192401.
7 F. Ibrahim, A. Hallal, A. Kalitsov, D. Stewart, B. Dieny and M. Chshiev, *Phys. Rev. Appl.*, 2022, **17**, 054041.
8 W. Lin, B. Yang, A. P. Chen, X. Wu, R. Guo, S. Chen, L. Liu, Q. Xie, X. Shu, Y. Hui, G. M. Chow, Y. Feng, G. Carlotti, S. Tacchi, H. Yang and J. Chen, *Phys. Rev. Lett.*, 2020, **124**, 217202.
9 B. S. Yang, L. N. Jiang, W. Z. Chen, P. Tang, J. Zhang, X. G. Zhang, Y. Yan and X. F. Han, *Appl. Phys. Lett.*, 2018, **112**, 142403.
10 B. Peng, Z. Zhou, T. Nan, G. Dong, M. Feng, Q. Yang, X. Wang, S. Zhao, D. Xian, Z. D. Jiang, W. Ren, Z. G. Ye, N. X. Sun and M. Liu, *ACS Nano*, 2017, **11**, 4337–4345.
11 Y. H. Chu, L. W. Martin, M. B. Holcomb, M. Gajek, S. J. Han, Q. He, N. Balke, C. H. Yang, D. Lee, W. Hu, Q. Zhan, P. L. Yang, A. Fraile-Rodríguez, A. Scholl, S. X. Wang and R. Ramesh, *Nat. Mater.*, 2008, **7**, 478–482.
12 V. Garcia, M. Bibes, L. Bocher, S. Valencia, F. Kronast, A. Crassous, X. Moya, S. Enouz-Vedrenne, A. Gloter, D. Imhoff, C. Deranlot, N. D. Mathur, S. Fusil, K. Bouzehouane and A. Barthélémy, *Science*, 2010, **327**, 1106–1110.
13 N. A. Spaldin and M. Fiebig, *Science*, 2005, **309**, 391–392.
14 W. Eerenstein, N. D. Mathur and J. F. Scott, *Nature*, 2006, **442**, 759–765.
15 N. A. Spaldin, S. W. Cheong and R. Ramesh, *Phys. Today*, 2010, **63**, 38–43.
16 S. Geprägs, A. Brandlmaier, M. Opel, R. Gross and S. T. B. Goennenwein, *Appl. Phys. Lett.*, 2010, **96**, 142509.
17 D. Odkhuu and N. Kioussis, *Phys. Rev. B*, 2018, **97**, 094404.
18 C. G. Duan, J. P. Velev, R. F. Sabirianov, Z. Zhu, J. Chu, S. S. Jaswal and E. Y. Tsymbal, *Phys. Rev. Lett.*, 2008, **101**, 137201.
19 G. Radaelli, D. Petti, E. Plekhanov, I. Fina, P. Torelli, B. R. Salles, M. Cantoni, C. Rinaldi, D. Gutiérrez, G. Panaccione, M. Varela, S. Picozzi, J. Fontcuberta and R. Bertacco, *Nat. Commun.*, 2014, **5**, 3404.

20 J. T. Heron, M. Trassin, K. Ashraf, M. Gajek, Q. He, S. Y. Yang, D. E. Nikonov, Y.-H. Chu, S. Salahuddin and R. Ramesh, *Phys. Rev. Lett.*, 2011, **107**, 217202.
21 J. T. Heron, J. L. Bosse, Q. He, Y. Gao, M. Trassin, L. Ye, J. D. Clarkson, C. Wang, J. Liu, S. Salahuddin, D. C. Ralph, D. G. Schlom, J. Íñiguez, B. D. Huey and R. Ramesh, *Nature*, 2014, **516**, 370–373.
22 J. M. Hu, T. Yang, J. Wang, H. Huang, J. Zhang, L. Q. Chen and C.-W. Nan, *Nano Lett.*, 2015, **15**, 616–622.
23 D. B. Gopman, P. Chen, J. W. Lau, A. C. Chavez, G. P. Carman, P. Finkel, M. Staruch and R. D. Shull, *ACS Appl. Mater. Interfaces*, 2018, **10**, 24725–24732.
24 S. Kokado, N. Fujima, K. Harigaya, H. Shimizu and A. Sakuma, *Phys. Rev. B: Condens. Matter Mater. Phys.*, 2006, **73**, 172410.
25 W. B. Mi, Z. B. Guo, X. P. Feng and H. L. Bai, *Acta Mater.*, 2013, **61**, 6387–6395.
26 Y. Komasaki, M. Tsunoda, S. Isogami and M. Takahashi, *J. Appl. Phys.*, 2009, **105**, 07C928.
27 Z. Lai, C. Li, Z. Li, X. Liu, Z. Zhou, W. Mi and M. Liu, *J. Mater. Chem. C*, 2019, **7**, 8537–8545.
28 Z. R. Li, X. P. Feng, X. C. Wang and W. B. Mi, *Mater. Res. Bull.*, 2015, **65**, 175–182.
29 Z. Lai, Z. Li, X. Liu, L. Bai, Y. Tian and W. Mi, *J. Phys. D: Appl. Phys.*, 2018, **51**, 245001.
30 Z. Lai, P. Li and W. Mi, *J. Appl. Phys.*, 2019, **126**, 113901.
31 Z. R. Li, W. B. Mi and H. L. Bai, *J. Phys. D: Appl. Phys.*, 2019, **52**, 335001.
32 B. Yang, L. Tao, L. Jiang, W. Chen, P. Tang, Y. Yan and X. Han, *Phys. Rev. Appl.*, 2018, **9**, 054019.
33 Z. Li, X. Wang, H. Dai, W. Mi and H. Bai, *Thin Solid Films*, 2015, **588**, 26–33.
34 X. Han, W. Mi and D. Wang, *J. Mater. Chem. C*, 2020, **8**, 3137–3146.
35 L. Yin, W. Mi and X. Wang, *Phys. Rev. Appl.*, 2016, **6**, 064022.
36 L. Yin, X. Wang and W. Mi, *ACS Appl. Mater. Interfaces*, 2017, **9**, 15887–15892.
37 L. Yin, X. Wang and W. Mi, *Appl. Phys. Lett.*, 2017, **111**, 032404.
38 Z. R. Li, W. B. Mi and H. L. Bai, *Appl. Phys. Lett.*, 2018, **113**, 132401.
39 Z. R. Li, W. B. Mi and H. L. Bai, *Comput. Mater. Sci.*, 2018, **142**, 145–152.
40 Z. R. Li, W. B. Mi and H. L. Bai, *ACS Appl. Mater. Interfaces*, 2018, **10**, 16674–16680.
41 L. Yu, G. Gao, G. Ding, Y. Duan, Y. Liu, Y. He and K. Yao, *RSC Adv.*, 2016, **6**, 29504–29511.
42 G. Kresse and J. Furthmüller, *Phys. Rev. B: Condens. Matter Mater. Phys.*, 1996, **54**, 11169.
43 G. Kresse and J. Hafner, *Phys. Rev. B: Condens. Matter Mater. Phys.*, 1993, **48**, 13115.
44 G. Kresse and J. Furthmüller, *Comput. Mater. Sci.*, 1996, **6**, 15–50.
45 J. Perdew, K. Burke and M. Ernzerhof, *Phys. Rev. Lett.*, 1996, **77**, 3865.
46 P. Ghosez and J. Junquera, *Annu. Rev. Condens. Matter Phys.*, 2022, **13**, 325–364.
47 N. Feng, W. Mi, X. Wang and H. Bai, *RSC Adv.*, 2014, **4**, 48848–48859.
48 D. Odkhuu, *Phys. Rev. B*, 2017, **96**, 134402.
49 G. H. O. Daalderop, P. J. Kelly and M. F. H. Schuurmans, *Phys. Rev. B: Condens. Matter Mater. Phys.*, 1990, **41**, 11919.
50 D. Wang, R. Wu and A. J. Freeman, *Phys. Rev. B: Condens. Matter Mater. Phys.*, 1993, **47**, 14932.
51 B. S. Yang, J. Zhang, L. N. Jiang, W. Z. Chen, P. Tang, X. G. Zhang, Y. Yan and X. F. Han, *Phys. Rev. B*, 2017, **95**, 174424.
52 A. Houari, S. F. Matar and M. A. Belkhir, *J. Magn. Magn. Mater.*, 2010, **322**, 658–660.
53 W. Wang, W. Sun, G. Zhang, F. Ren, Y. Wang, C. You and Z. Cheng, *J. Adv. Res.*, 2020, **24**, 371–377.
54 M. Zhao, C. Jin, W. Sun, W. Zhai, F. Ren and B. Wang, *Results Phys.*, 2022, **37**, 105538.
55 C. G. Duan, S. S. Jaswal and E. Y. Tsymbal, *Phys. Rev. Lett.*, 2006, **97**, 047201.